Modeling Method for Semi-crystalline Polymers Controlling Aspects of the Morphology at the Molecular Scale for the Study of Mechanical and Physicochemical Properties

Boris Belin, Marianna Yiannourakou, Véronique Lachet, Bernard Rousseau

A modeling method for semi-crystalline polymers controlling aspects of the morphology at the molecular scale for the study of mechanical and physico-chemical properties

Boris Belin,[†,‡,¶] Marianna Yiannourakou,[¶] Véronique Lachet,[‡] and Bernard Rousseau[*,†]

[†]*Université Paris Saclay, CNRS, Institut de Chimie-Physique UMR 8000, 91405 Orsay, France*

[‡]*IFP Energies nouvelles, 92852 Rueil-Malmaison, France*

[¶]*Materials Design SARL, 92120 Montrouge, France*

E-mail: bernard.rousseau@cnrs.fr

Abstract

A novel method is presented to build semi-crystalline polymer models used in molecular dynamics simulations. The method allows controlling certain aspects of the molecular morphology of the material. It relies on the generation of the polymer sections in the amorphous phase of the semi-crystalline structure according to the statistical polymer physics theory proposed by Adhikari and Muthukumar.[1] The amorphous phase is first built based on the method initially developed by Theodorou and Suter.[2] Then, the amorphous phase is stacked between crystallites, and a connection algorithm proposed by Rigby et al.,[3] initially developed to build polymer thermosets, is employed to link two phases. For a given set of crystallinity degree, semi-crystalline long period, densities of the crystalline and amorphous phases and polymer molecular weight, the characteristic ratio is used to control the relative fractions of different types of polymer sections in the amorphous phase as well as the distribution of their lengths. There are three types of amorphous polymer sections: the ones that are reentering in the same crystallite called loops, those that are bonding two different crystallites called tie chains, and the chain tails ending in the amorphous region. The higher this characteristic ratio is, the higher the fraction of tie chains is. The full implementation of the theory is described and then applied to High-Density PolyEthylene (HDPE). Several samples are generated. The obtained structures are characterized. Their elastic coefficients are computed, and high uniaxial deformations are performed. It is shown that the higher the crystallinity degree, the higher the elastic coefficients. An entanglement analysis shows that the quantity of tie chains is more decisive than the entanglements in acting as stress transmitters to rigidify the structure.

1 Introduction and state of the art

Polymers can be manufactured into various shapes by a variety of industrial processes like molding, thermoforming, 3D printing, making them ubiquitous.[4] Many industries are using them for their mechanical, permeation, dielectric, optical, thermal, and chemical properties, among others.[5] Polymers can solidify into vitreous or crystalline states but may also adopt a semi-crystalline structure. However, the complete morphology of the semi-crystalline structure, with organization at different length scales, is still not fully understood. With the help of material simulations, the present work aims to elucidate how the morphology influences the physico-chemical properties to design better materials and comprehend those micro-structures at the fundamental level. While our study uses a polyethylene (PE) model, the methodology is generic enough to be used for other semi-crystalline polymers. We focus on model constructions at the molecular scale, the description of the obtained morphologies and the computation of their mechanical properties.

In the 1970s, the path of a single deuterated polyethylene chain in the bulk semi-crystalline structure obtained by quenching from the melt was studied with neutron scattering (NS).[6–9] It was shown that the radius of gyration of the polymer in the semi-crystalline structure is of the same length as the one in the melt, suggesting that the shape of the molecules is not strongly modified by the crystallization process giving rise to the formation of a low proportion of adjacent chain reentries (see figure 1 for definitions). On the other hand, the radius of gyration in the solution-grown pure polyethylene crystal is much smaller, suggesting a high proportion of adjacent reentries,[10] hence a more regular and compact chain folding. In addition, folding patterns of deuterated chains in the solution-grown single-crystals were studied using infrared spectroscopy (IR) and it was also concluded that a high proportion of adjacent reentries[11–14] exists, in agreement with the NS measurements. Since the 2000s, new techniques were used to characterize the morphology: atomic force microscopy (AFM) and solid-state nuclear magnetic resonance (ss NMR), the latter also relying on isotope labeling of a small proportion of the chains. AFM images of polymer

semi-crystalline films of isotactic poly(methyl methacrylate)[15] and polyethylene[16,17] allowed to conclude to a high proportion of adjacent reentries contrary to the NS measurements on semi-crystalline material obtained from the melt. Ss NMR[18,19] studies showed a high proportion of adjacent reentries on polypropylene solution-grown single-crystals and polypropylene semi-crystalline obtained from the melt, adding the additional results that the morphology was less dependent from the kinetic path to crystallization than from the entanglements in the initial amorphous material. As we can see, results are still controversial depending on the specific polymer and the sample type: single-crystal, semi-crystalline from the melt or films. There is still a controversy regarding the fraction of adjacent reentries and lengths of other folding or bridging patterns. The sample specific preparation for each experiment and the limitations of the characterization methods are introducing biases.

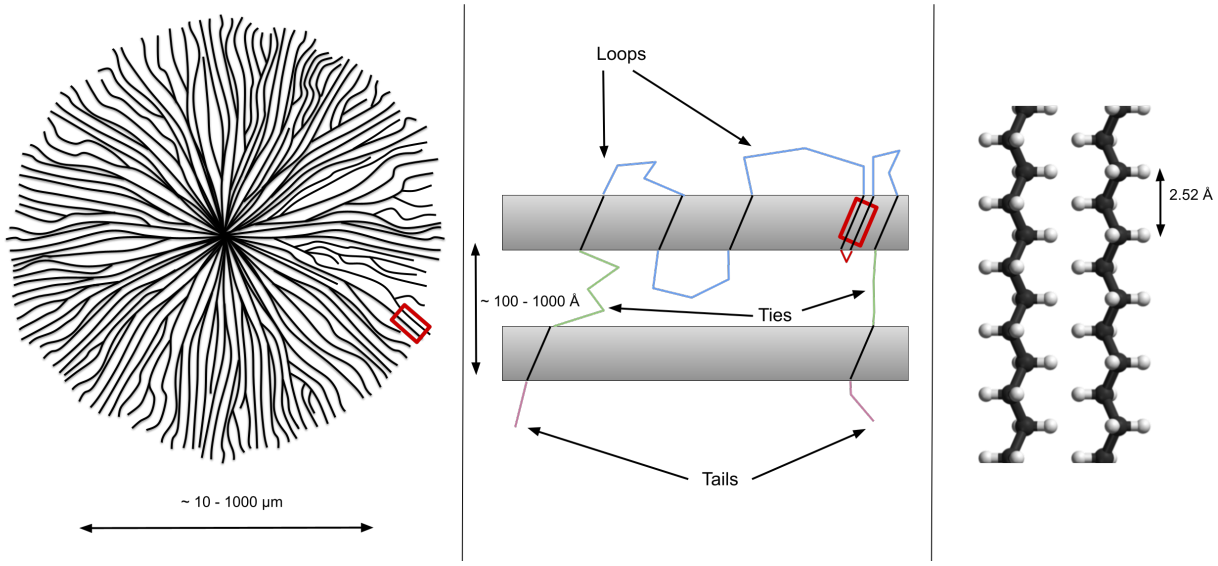

Figure 1: "Multiscale" scheme of semi-crystalline polymers. Left: a micron-sized spherulite consisting of crystalline lamellae emanating from a nucleation center in all directions. These lamellae are aligned polymers forming a crystalline region. Middle: a single polymer chain is represented crossing two lamellae in grey, the walks in the amorphous regions are of three types: loops in blue, the polymer is reentering the same lamella, bridge or tie chains in green, the polymer is bonding two lamellae, and tails in purple, the polymer ends in the unordered phase. The red walk is called an adjacent reentry, also called a perfect fold. This is the smallest possible loop. Right: a representation of two crystalline paralleled polyethylene chains. The red rectangles show the successive magnification from left to right.

Molecular modeling has been employed to simulate nucleation from the melt with molec-

ular dynamics.[20–35] Those simulations provide valuable information about the process of nucleation at the molecular scale, helping to understand the nature of the chain foldings composing the crystallites. However, observing direct nucleation using molecular dynamics is challenging because homogeneous nucleation is a rare event, anisotropic, necessitating the concomitant creation of a surface normal to the direction of the chains and the lateral stacking of parallel chains.[24] Simulations have to be biased to accelerate the creation of a nucleus large enough to survive and grow in an accessible simulation time. Biases include the use of super-cooled short chains,[20–25] pre-oriented chains,[26–29] artificially stiffened chains.[30,31] Coarse-graining[32–36] was also used to speed up the simulation. Moreover, the small size of the simulation boxes (≈ 100 Å) limits the apparition of the characteristic lamellar structure observed in experiments *i.e.* the regular alternation of crystalline and amorphous phases (see the middle image of figure 1). Thus the obtained systems are inappropriate for property calculations. Therefore different procedures were proposed in the literature to build directly semi-crystalline structures.

Balijepalli *et al.* proposed in 1998 the *Interphase Monte Carlo* method[37–42] hereinafter referred to as the Rutledge model. The method starts with a cuboid of pure crystal. In a middle section of the cuboid, intended to become the amorphous phase, monomers or large chain segments are deleted according to the target density of the amorphous region. Then, a Monte Carlo procedure of slicing chain bonds, connecting chain ends, and classic displacement-type moves of the chains is performed in the central cuboid section. Nilsson *et al.* in 2012 proposed the *Monte Carlo random walk model*.[43] This method creates chain segments in the amorphous region using a random walk between two crystallites. When the random walk reaches a crystallite, it automatically connects to a crystalline stem (chain segment organized according to the crystallographic structure). The chains are emerging from the lamellae and are folded back adjacently or are initiating a random walk forming loops or tie chains (see figure 1). The target amorphous phase density is achieved by adjusting the number of direct adjacent reentries. The methods of Nilsson and Rutledge use the

amorphous phase density as the controlling parameter plus random walks or a Monte Carlo connection algorithm.

Pandiyan and Rousseau[44] proposed to start with a pure crystalline sample and to randomly cut each chain in a central region followed by a relaxation above the melting temperature to create a disordered region while keeping atoms in crystalline regions at a fixed position. Two chain ends are then connected during a relaxation, creating a chemical bond when falling within a cut-off distance. The connections are accepted or rejected according to the fractions of polymer section types given as input. This method allows the investigation of the role of each kind of polymer section (tie chains, loops, and tails) controlling their relative fractions.[44] Starting with information about the morphology instead of starting with the density as the controlling parameter was also proposed by Monasse and Queyroy,[45,46] who chose specific reference systems with a complete morphology given as input and directly built the structures "by hand".

Nilsson and Rutledge's methods do not control the morphologies. Nilsson's *Monte Carlo random walk model* relies on a high proportion of adjacent reentries to obtain the experimental density of the amorphous phase; this is a debatable choice looking at the experimental literature. In Pandiyan *et al.* work,[44] a large number of chains were not connected, resulting in an unrealistic high number of tails and thus a simulation box with unrealistically low molecular weight molecules. Monasse and Queyroy construction is laborious; one has to know all the morphological traits of the structure before building it and place monomers one by one in the simulation cell, which is not convenient for systematic studies of semi-crystalline samples.

When looking for a building method convenient to treat the relationship between the morphology and the physico-chemical properties, three main criteria may be defined:

- The method has to be automated or automatable to generate multiple cells in a limited amount of time.

- Some control on the morphologies is necessary.

- The method has to have intrinsic randomness to build different models with the same morphological characteristics as input.

Here, we propose a method to generate an amorphous region respecting statistics for the type of chain section fractions, and their lengths, and then connect the amorphous region between two crystallites. Such a method requires a statistical theory of chain behavior in the amorphous phase. The pioneer theory for the statistical physics of semi-crystalline polymers was the gambler's ruin model.[47] Like the Nilsson *Monte Carlo random walks*, this theory has the inconvenience of using the adjacent reentries to correct the density. The statistics of ties, loops, and tails published by Adhikari[1] in 2019 is a new proposition. Adhikari's work also relies on random walks in a polymer field-theoretic formalism but avoids the necessity of a correction with adjacent reentries. The formalism relies on the freely jointed chain. The segments of the freely jointed chains have the same length and are directed toward a random direction. Changing the segment length of the freely jointed chain controls the morphology: the more a chain emerging from the crystalline phase persists in its direction, i.e. the larger the chain rigidity, the more the probability for the chain to dive in the opposite crystalline phase is high thus giving rise to a high tie chain fraction. Changing the proportion of chain segments in the amorphous section allows to study their influence on the mechanical properties. By studying systems with different crystalline fractions and different tie fractions, we can access the effect of morphological differences on semi-crystalline polymer properties. Moreover, an entanglement analysis is performed to understand what is the more decisive factor regarding the mechanical properties, entanglements or chain section types.

The paper is organized as follows. In section 2 we briefly present the statistical theory proposed by Adhikari and Muthukumar[1] to obtain the fraction of tie segments and the length distribution of tie, loop and tail segments. Then we explain how this theory is used to build real models of semi-crystalline polymers. In section 3, we present our results starting with information regarding final morphologies of the samples, their elastic properties and finally their behavior under large uniaxial deformations. We finally give a conclusion and suggest

some future work in this area.

2 Methods

2.1 Theory of statistics of ties, loops and tails in semi-crystalline polymers

In this section, we briefly recall Adhikari and Muthukumar theory.[1] Please refer to the original paper for a detailed presentation of this work. Adhikari and Muthukumar theory enables to study the statistics of ties and loops for a reference chain of finite length allowing its connectivity to multiple lamellae. It is assumed that polymer chains in amorphous regions are in the equilibrium state and follow Gaussian statistics. Ties, loops and tails are obtained from a three-dimensional random walk between "absorbing" walls. The walk of the reference polymer chain starts at a point in an amorphous region until it touches a lamellar surface, forming a first chain end, here referred to as a tail. Once the chain touches a lamellar surface, the formation of a rigid and vertical crystalline stem is guaranteed. Then, the chain emerges out of the crystalline lamella and enters into the other amorphous region. The random walk is pursued, giving rise to loops or ties until the reference chain ends in the amorphous region. By allowing the length of tails, loops and ties to vary, Adhikari and Muthukumar calculate the probability of formation of a chain of length N with a number of ties n_{tie} when n_{stem} exist, associated with an arbitrary number of lamellae and amorphous regions. Such probability is given as:

$$Z(n_{\text{tie}}, n_{\text{stem}}, N) = \mathcal{L}^{-1}[(\tilde{g}_{\text{tail}}(E))^2(\tilde{g}_{\text{tie}}(E))^{n_{\text{tie}}}(\tilde{g}_{\text{loop}}(E))^{n_{\text{stem}}-n_{\text{tie}}-1}] \tag{1}$$

where $\mathcal{L}^{-1}$ is the inverse Laplace operator and $\tilde{g}_{\text{tie}}(E)$, $\tilde{g}_{\text{tail}}(E)$ and $\tilde{g}_{\text{loop}}(E)$ are the Laplace transform of $g_{\text{tie}}(s)$ the probability of formation of tie of length s and similarly for $g_{\text{tail}}(s)$ and $g_{\text{loop}}(s)$. The final expression for the probability (including a typo correction from Adhikari

and Muthukumar paper) is:

$$Z(n_{\text{tie}}, n_{\text{stem}}, N) = \mathcal{L}^{-1}\left[\left(\frac{1}{E} - \frac{\sinh\left(\sqrt{\frac{E}{D}}\right)}{E\sinh\left(d'\sqrt{\frac{E}{D}}\right)} - \frac{\sinh\left((d'-1)\sqrt{\frac{E}{D}}\right)}{E\sinh\left(d'\sqrt{\frac{E}{D}}\right)}\right)^2 \times \left(\frac{\sinh\left(\sqrt{\frac{E}{D}}\right)}{\sinh\left(d'\sqrt{\frac{E}{D}}\right)}\right)^{n_{\text{tie}}} \left(\frac{\sinh\left((d'-1)\sqrt{\frac{E}{D}}\right)}{\sinh\left(d'\sqrt{\frac{E}{D}}\right)}\right)^{n_{\text{stem}}-n_{\text{tie}}-1}\right] \quad (2)$$

($D = 1/6$ in our study) and d' is the intercrystalline length expressed in Kuhn length units. The fraction of tie segments is thus obtained from the probability $Z(n_{\text{tie}}, n_{\text{stem}}, N)$. When the number of stems formed is n_{stem}, the number of ties can vary from zero to $n_{\text{stem}}-1$. Also, for a fixed number of stems, there are different ways of forming a given number of ties. Then, the average number of ties formed per molecule, $\bar{n}_{\text{tie}}$ is given by:

$$\bar{n}_{tie} = \frac{\sum_{n_{tie}=0}^{n_{stem}-1} \omega_{n_{\text{tie}}} n_{tie} Z(n_{tie}, n_{stem}, N)}{\sum_{n_{tie}=0}^{n_{stem}-1} \omega_{n_{\text{tie}}} Z(n_{tie}, n_{stem}, N)} \quad (3)$$

where $\omega_{n_{tie}}$ is the number of ways of forming n_{tie} ties when the total number of ties and loops per molecule is $n_{\text{stem}} - 1$, which is:

$$\omega_{n_{\text{tie}}} = \frac{(n_{\text{stem}}-1)!}{n_{\text{tie}}!(n_{\text{stem}}-1-n_{\text{tie}})!} \quad (4)$$

Finally, the fraction of ties f_{tie} is given by:

$$f_{tie} = \frac{\bar{n}_{tie}}{n_{\text{stem}}+1} \quad (5)$$

Knowing the average number of tie chains per molecule, we obtain the average number of loop chains per molecule as $\bar{n}_{\text{loop}} = n_{\text{stem}} - 1 - \bar{n}_{\text{tie}}$. Obviously, the number of tail segments per molecule is $n_{\text{tail}} = 2$.

2.2 Semi-crystalline samples construction

In this section, we present how we apply Adhikari and Muthukumar theory to the construction of semi-crystalline samples for molecular dynamics study. Computing the fraction of ties using Adhikari and Muthukumar theory requires a small amount of input data: the reference chain length N, the amorphous thickness d and the crystalline lamellar thickness m. The last two quantities are obtained using the degree of crystallinity χ. In[1] it was assumed equal density of the crystalline and amorphous phases. Length distribution of ties and loops in Kuhn segment length and ties fractions are finally obtained from the theory.

In this work, we want to build semi-crystalline samples at the atomistic length scale and provide a methodology applicable to different polymers. Our input parameters must thus use some quantities specific of the polymer to model. We also need to account for accessible computing ressources which give a limit to system sizes. Finally, we would like to define some control parameter(s) which alters the fraction of ties and loops in the amorphous regions for a given semi-crystalline degree.

The mass crystallinity degree χ is one of the most important parameter here. Together with the so-called long period L_p, i.e. the period of amorphous and crystalline phases alternation, a length scale can be obtained. We build molecular simulation boxes containing two such periods, which means that the box initially contains two crystalline lamella separated by amorphous regions along the z direction. Full periodicity of the box is assumed in all three directions. The simulation box contains two polymer chains. Each crystalline region is built using primitive cell informations[48] with an integer number of primitive cells in the x and y directions. The number of unit cells in the x and y directions imposes the initial number of stems in the system. The total number of crystalline cells in the z direction is

computed from the length of the crystalline regions m. For PE, each unit cell in the xy plane contains two crystalline stems.

Contrarily to the work of Adhikari and Muthukumar, we want to account for the difference between amorphous and crystalline densities, ρ_a and ρ_c respectively, where ρ_a is the average density of the non-crystalline domain taking into account the interphase. ρ_a was taken to be equal to 0.91 g/cm^{-3}. ρ_c is computed from unit cell dimensions.

From the definition of the long period:

$$L_p = m + d \,, \tag{6}$$

and from the crystallinity degree:

$$\chi = \frac{\rho_c m}{\rho_c m + \rho_a d} \,, \tag{7}$$

we get values for m and d thicknesses:

$$m = \frac{\chi L_p}{\chi + (1-\chi)(\rho_c/\rho_a)} \,, \tag{8}$$

$$d = \frac{(1-\chi) L_p}{\chi(\rho_a/\rho_c) + (1-\chi)} \,. \tag{9}$$

The Kuhn length is obtained from the knowledge of the characteristic ratio C_∞, an intrinsic property of a polymer, and the backbone geometry. For polyethylene, we have:[49]

$$b = \frac{C_\infty l}{\cos(\theta/2)} \tag{10}$$

where l is the carbon-carbon bond length and $\pi - \theta$ is the angle between two adjacent

bonds along the polymer backbone.

The conversion from n, the number of CH_2 groups to N, the number of Kuhn segments is:

$$N = \frac{n \cos^2 \frac{\theta}{2}}{C_\infty} . \tag{11}$$

From the total density ρ and the simulation box size we obtain the chain molecular weight M_w. Parameters are related quantities are given table 1. The last parameter to be fixed is

Table 1: Parameters used to build semi-crystalline samples with $\chi = 0.5$ and 0.7. Also indicated the density of the boxes and the molecular weight of each molecule in the final structures.

l (Å)	1.54	
θ (°)	68	
n_{stem}	70	
ρ_a (g/cm^3)	0.91	
ρ_c (g/cm^3)	1	
L_p (Å)	200	
χ	0.5	0.7
ρ (g/cm^3)	0.955	0.973
M_w (g/mol)	149432	147668

the characteristic ratio C_∞. The characteristic ratio computed by Flory is 6.9 at 413 K.[50] As presented in the introduction, the length of the freely jointed segment, i.e. the Kuhn length, has an influence on the fraction of ties in the system, f_{tie}. Thus, by changing the value of the characteristic ratio we can control the relative fractions of type of walks keeping the other parameters identical. We believe that the chains in the amorphous regions are more constrained than in a bulk amorphous system. Plus, the characteristic ratio was obtained in the melt, at high temperature. We thus expect that $C_\infty = 6.8$ is a lower bound for the characteristic ratio describing chain segments in a semi-crystalline sample. Different characteristic ratios: $C_\infty = 7$, 9, 11 and 13, will be used to generate the structures at two different crystallinity ratio $\chi = 0.5$, 0.7. The corresponding fractions of tie chains are plotted figure 2.

For each structure, we compute the number of tie, loop, and tail chains. We determine

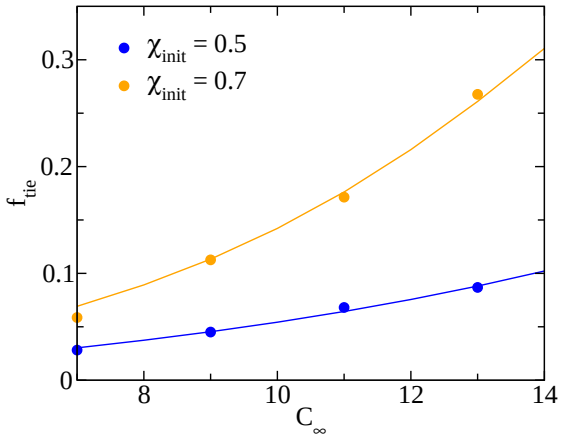

Figure 2: Fraction of tie chains, $f_{\rm tie}$, as a function of the characteristic ratio C_∞ as obtained from the theory (full lines) and for the samples built in this study (symbols) for the two crystalline ratios studied here.

the length distribution of the chain sections in the amorphous phase using the probability distributions $g_{\rm tie}$, $g_{\rm loop}$ and $g_{\rm tail}$. The distributions have to be truncated as in Adhikari formalism, they are not bounded toward $s \to +\infty$. In a real system, chain extension must be limited to the physical space allowed between crystalline regions. A coarse way to obtain a range $[1, P]$ of Kuhn segments to bound the probability distribution is to consider the weighted average of the length of tie, loop and tail chains in Kuhn segments: $s^P_{\rm tie}$, $s^P_{\rm loop}$ and $s^P_{\rm tail}$ and to write the following identity concerning the number of amorphous Kuhn segments $N_a = (1-\chi)N$.

$$N_a = \bar{n}_{\rm tie} s^P_{\rm tie} + \bar{n}_{\rm loop} s^P_{\rm loop} + 2 s^P_{\rm tail} \; . \tag{12}$$

$$N_a = \bar{n}_{\rm tie} \sum_{s=1}^{P} g^P_{\rm tie}(s) \times s + \bar{n}_{\rm loop} \sum_{s=1}^{P} g^P_{\rm loop}(s) \times s + 2 \sum_{s=1}^{P} g^P_{\rm tail}(s) \times s \; , \tag{13}$$

where the g^P_i are the final probabilities used in this study:

$$g^P_{\rm tie}(s) = \frac{g_{\rm tie}(s)}{\sum_{s=1}^{P} g_{\rm tie}(s)} \; , \tag{14}$$

$$g^P_{\rm loop}(s) = \frac{g_{\rm loop}(s)}{\sum_{s=1}^{P} g_{\rm loop}(s)} \; , \tag{15}$$

$$g_{\text{tail}}^{P}(s) = \frac{g_{\text{tail}}(s)}{\sum_{s=1}^{P} g_{\text{tail}}(s)} \ . \tag{16}$$

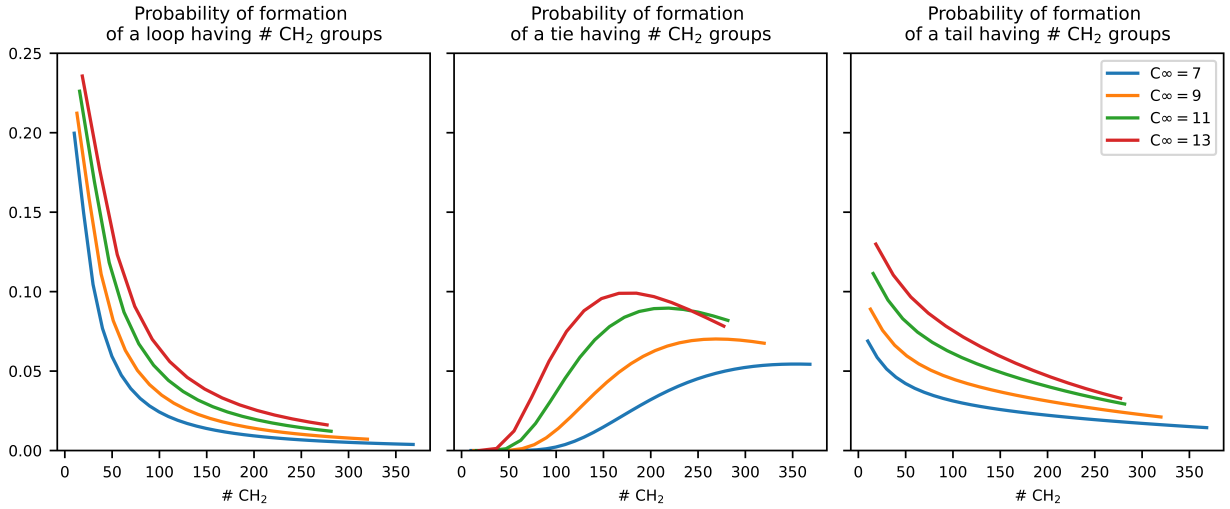

Figure 3: Final probabilities of formation of tie chains, loops and tails for $\chi = 0.5$ and different values of C_∞.

We find the correct P which gives the correct average number of amorphous segments N_a. Those probabilities are discret probabilities of the number of Kuhn segments per walk in the amorphous phase. From equation (11), we express the length of the walks in the amorphous phase according the number of atoms in the backbone: $n = \frac{NC_\infty}{\cos^2 \theta/2}$. We do not want to have only multiples of $\frac{C_\infty}{\cos^2 \theta/2}$ for n, thus we interpolate the cumulative distribution functions of the probability distribution functions (14), (15), (16) and a procedure called *Inverse Transform Sampling* was used to randomly pick a number from those non-analytical numerical probability distributions (see figures 3 and 4). This procedure is well described in this reference.[51] It allows to pick a number according to a discrete probability distribution as if it was a continuous function.

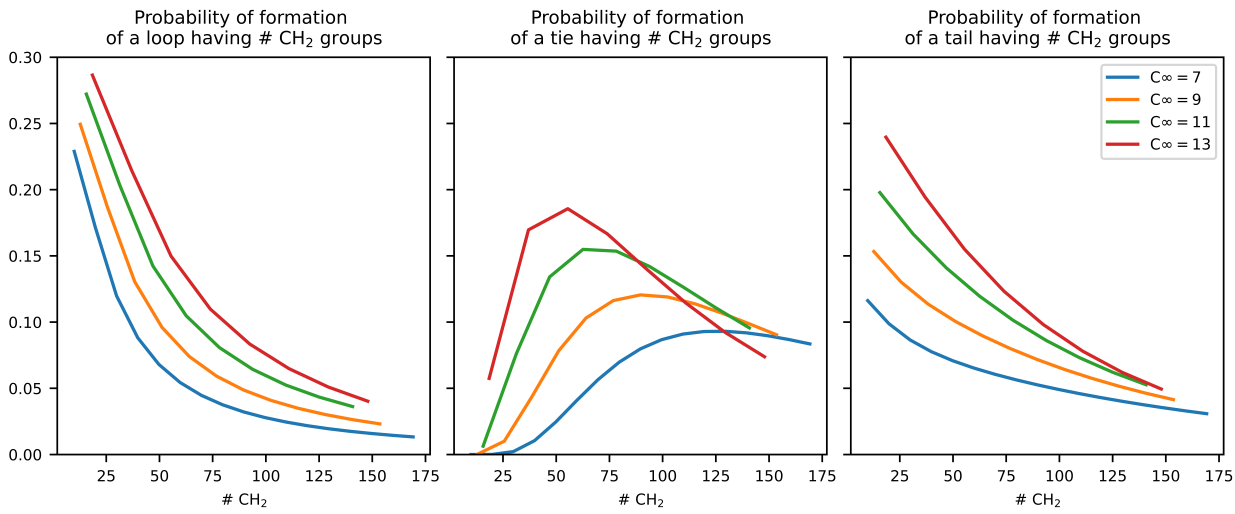

Figure 4: Final probabilities of formation of tie chains, loops and tails for $\chi = 0.7$ and different values of C_∞.

2.3 Connection algorithm and molecular dynamics

For each structure, we build the crystalline phases using unit cell information and box and region dimensions. We build two amorphous phases using the MedeA Amorphous Materials Builder[52] which is based on the work by Theodorou and Sutter algorithm[2] with the chain sections taken in the probability distributions. The crystalline and the amorphous regions are then stacked together. We label the ends of the chain segments in the amorphous phases according to the desired connections. A tie chain will have one end labeled A and the other B, a tail chain will have one of the ends only labeled A or B, loop chains will have both ends labeled with the same letter A or B. The reactive sites (CH_3) on one edge of the crystallite stems are labelled C and those on the other edge D. Then a connection algorithm is launched, originally designed for thermoset building.[3] The algorithm is a tool of the material simulation software MedeA,[52] and is named Thermoset builder. Spheres of capture centered on the labeled site grow incrementally with a chosen step. Every time it meets an allowed connection (here A with C and B with D) it forms a bond, and performs a few steps of an NVT relaxation. We keep the crystalline phases frozen during the connection process. We obtain structures like the one on the figure 5. The structures were thermalized

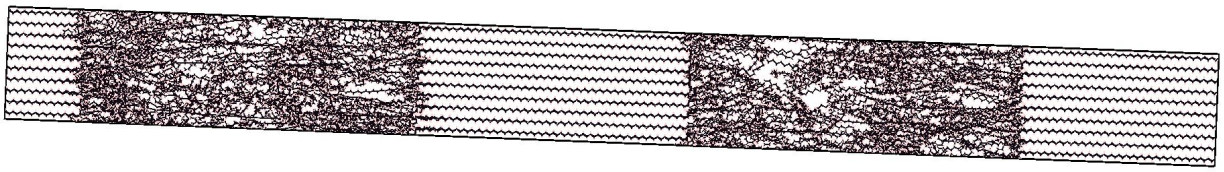

Figure 5: Structure with crystallinity degree $\chi = 0.5$ after connection and before relaxation.

and mechanically equilibrated during 100 ns with LAMMPS[53] and the forcefield TraPPE-UA[54] in the NPT ensemble with $T = 300$ K and $P = 1$ atm with a time step of 1 fs (see fig. 6). The NPT ensemble used here allows relaxation in each spatial direction to ensure correct equilibration of box lengths in all directions (known as LAMMPS NPT *aniso* mode).

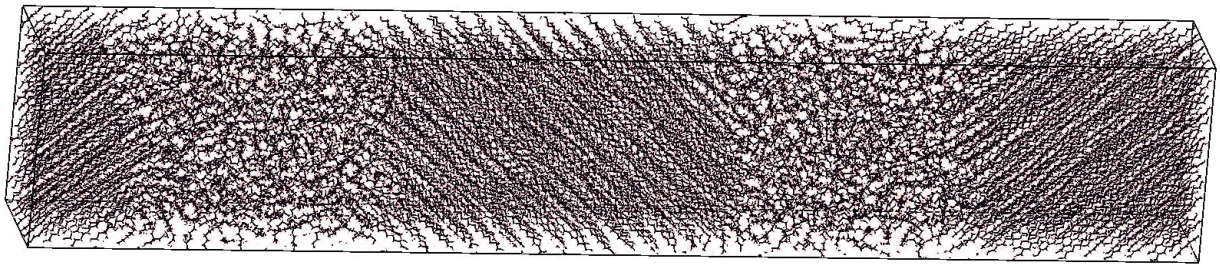

Figure 6: Structure with an initial crystallinity degree $\chi = 0.5$ after relaxation.

3 Results

3.1 Structural characterization of the samples

In this work, 27 structures, i.e. 27 simulation boxes, were generated with different crystallinity degrees and characteristic ratios (see table 2).

Table 2: Number of modeled structures for each χ_{init} and C_∞.

	$\chi_{init} = 0.5$	$\chi_{init} = 0.7$
$C_\infty = 7$	3	3
$C_\infty = 9$	6	3
$C_\infty = 11$	3	3
$C_\infty = 13$	3	3

For all these structures, the crystallinity degree after relaxation was computed from the density profile along the z axis, normal to the amorphous-crystalline interface (see figure 7). A region is considered as amorphous when its density is smaller than 95% the crystalline density value, else it is considered as crystalline. After the NPT relaxation process, the average crystallinity is close to the initial one. Average values over all structures and corresponding standard deviations are given in table 3. Some fluctuations are observed, although the final crystallinity degree remains within two standard deviations. Semi-crystalline density after relaxation was also computed for all structures. Values are close from HDPE experimental data: 0.941-0.965g/cm^3.[55] As expected, a strong correlation can be seen between crystallinity degree and density (see figure 8).

Table 3: Mean of the crystallinity degrees $\overline{\chi}_{relax}$, and of the densities $\bar{\rho}_{relax}$ after relaxation, as well as their standard deviations $\sigma_{\chi_{relax}}$ and $\sigma_{\rho_{relax}}$.

χ_{init}	0.5	0.7
$\overline{\chi}_{relax}$	0.49	0.67
$\sigma_{\chi_{relax}}$	0.05	0.06
$\overline{\rho}_{relax}$	0.939	0.966
$\sigma_{\rho_{relax}}$	0.008	0.006

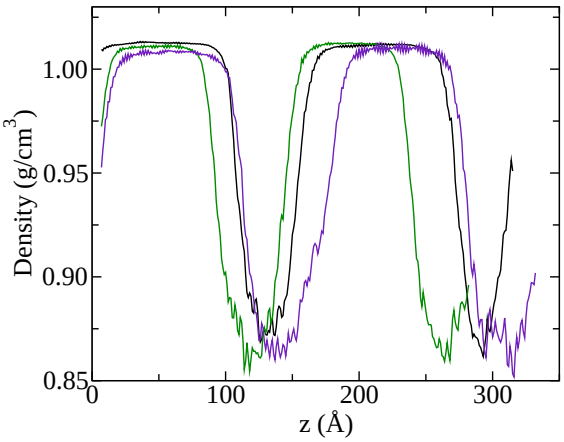

Figure 7: Density profile along the z axis, the axis of the long period, of the 3 structures with $\chi_{init} = 0.7$ and $C_\infty = 7$.

Thus, we have observed that our structures respect the original contraints imposed by the building procedure for macroscopic observables. We now turn to the analysis of the

molecular morphology of the samples, i.e. the amount of the different segment types and an entanglement analysis. Figure 2 shows that the expected fraction of ties is well reproduced for each crystallinity at every C_∞ value. The building procedure thus allows a fine control of the imposed structural constraints. Occasionally some connection cannot be performed. However this does not change significantly the imposed characteristics. Regarding the distributions of the size of the loops, contrary to Nilsson's samples[43] or Monasse and Queyroy's ones,[45] our structures have fewer small loops, i.e. adjacent reentries, roughly 1 to 2 per crystallite edge. As discussed in the introduction, the experimental literature shows that the amount of adjacent reentries may vary significantly depending on both the investigated samples and the employed characterization techniques. Thus, it is difficult to rely on this morphological parameter to conclude on the reliability of the procedure. The Z1 code

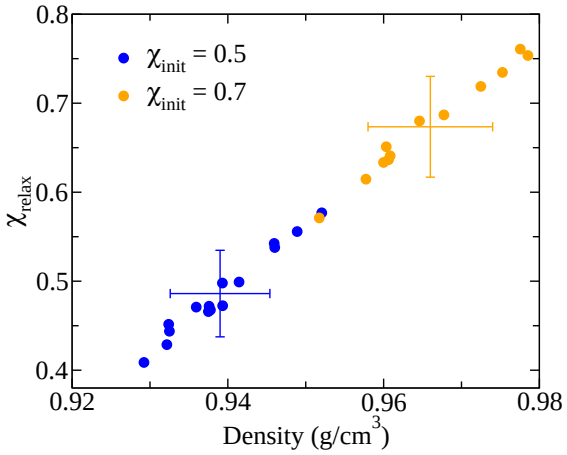

Figure 8: Crystallinity degree as a function of density for all studied structures. Blue and orange symbols correspond to structures with $\chi_{init} = 0.5$ and $\chi_{init} = 0.7$ respectively. The two crosses indicate the average crystallinity and average density with corresponding standard deviation.

from Martin Kröger[56] is used to analyze the entanglements in the amorphous phases of each structure in a similar way that Ranganathan et al.[57] did on their semi-crystalline structures. The obtained primitive paths for a typical structure is shown in figure 9. The primitive path of a polymer chain immersed in a space of obstacles (usually other polymers) is defined as the shortest path connecting the ends of the chain that does not violate the crossing of the

Figure 9: Primitive path of chains in an amorphous region computed with the Z1 code,[56] the segments belonging to loops are yellow and red, the segments belonging to tie chains are blue, the tail segments are in green. The spheres represent the primitive path kinks and the ends of the chains.

polymer chain.[58] After relaxation, the density of topological entanglements, defined as the number of links between two chain sections along their primitive path per unit volume of amorphous phase, is identical for all crystallinity degree values, as shown in figure 10. An average value around 0.78 entanglements per nm^3 is found, close to the value of 0.64 ± 0.03 nm^3 obtained by Lee and Rutledge.[59] However, comparison with experimental data suggests that amorphous region in semi-crystalline is more entangled than amorphous melt. The relationship between crystallization and entanglement is still a matter of debate. Assuming slow kinetics of crystallization, Hoffman and Miller[60] consider that entanglements are eliminated from the amorphous regions as crystallization proceeds, while Flory and Yoon[61] consider that chains cannot disentangle on the timescale of crystallization and entanglements are segregated into the amorphous domains. In the Flory and Yoon picture an increase of the density of entanglements in the amorphous phase is expected as crystallization proceeds. In the view of Hoffman and Miller, some fraction of entanglements should disappear during crystallization and the resulting entanglement density should be lower than expected from Flory and Yoon approach. This view is re-enforced by Bartczak's experimental work[62] who showed that a part of the entanglements was resolved during the crystallization depending

on the chain length and their irregularities like branches; an increase of chain length and irregularities both preventing the entanglement disparition. In our case, the large value of the entanglement density is rather in favor of Flory and Yoon theory, although the process involved to reach the semi-crystalline state is unphysical (building procedure rather than crystallization from the melt). The relevant point here is that the entanglement density should be larger than in the melt, a condition fulfilled by our building procedure.

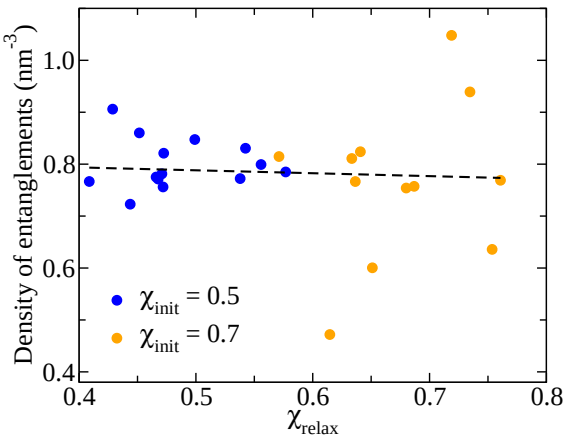

Figure 10: Density of topological entanglements in the amorphous regions as a function of the crystallinity degree χ_{relax} in all the generated semi-crystalline structures.

The entanglement length expressed in terms of number of CH_2 groups is evaluated with two estimators by the Z1 code: the classical kink entanglement length Ne_{CK} and the classical coil entanglement length Ne_{CC} defined in.[63] Averaged entanglement lengths are given in table 4 along with the corresponding entanglement weights W_e^a. Experimental data for entanglement weight in the melt is[64] $W_e^{melt} \approx 800$ to 1200 g/mol, a value two to three times larger than the one observed in our simulations though in agreement with the increase in entanglement density.

3.2 Elastic constants

The study focused on the three uniaxial coefficients of the elastic matrix c_{11}, c_{22} and c_{33}. All structures were strained with an engineering tensile strain of $\epsilon = \pm 1\%$ and $\pm 2\%$. The

Table 4: Mean and standard deviation over all structures of two different estimators developed by Kröger[56] for the entanglement lengths in amorphous domains expressed in number of CH_2 groups and in molecular weights.

	Ne_{CK}	Ne_{CC}
mean	23.6	28.9
standard deviation	3.7	7.9
W_e^a (g/mol)	330.5	405.9

results are shown figure 11. As expected from experimental studies,[65] the elastic coefficients increase with the crystallinity degree. The elastic coefficient c_{22} is higher than the c_{11} and c_{33} coefficients. In order to understand why the c_{22} coefficient is slightly larger than c_{11} and

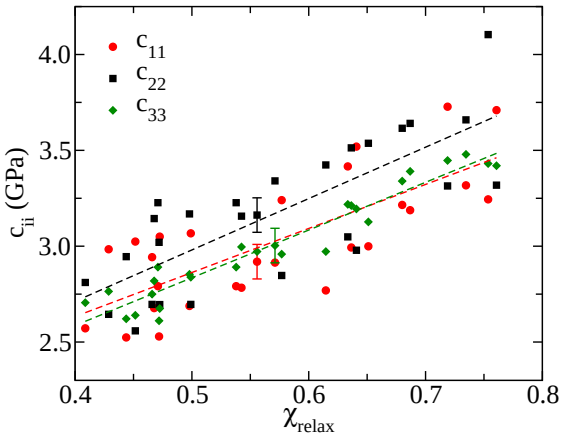

Figure 11: Tensile elastic coefficients c_{ii} as a function of the crystallinity degree χ_{relax} of all the modeled structures. Error bars represent statistical errors and are represented once for each coefficient.

c_{33}, is it important to look at the orientation of the structures relatively to the deformation direction. As shown figure 12, crystalline stems are tilted in the yz plane while there are normal to the x axis and parallel to the z axis in the xz plane.

When the sample is strained along the x or y directions, both crystalline and amorphous regions undergo the same deformation amplitude which imposes a deformation of the crystalline regions. A deformation along the x axis mostly implies changes of van der Waals interaction while a deformation along the y axis also implies changes of covalent interactions. The latter being stronger, c_{22} is expected to be larger than c_{11}. When the strain is applied

along the z axis, crystalline and amorphous regions undergo different deformation amplitudes and the elastic coefficient value c_{33} is mainly controlled by the elasticity of the soften region, i.e. the amorphous phase. This implies mostly changes in van der Waals interaction leading to a c_{33} value lower than c_{22}. In sum, when the structures are stretched in the z and

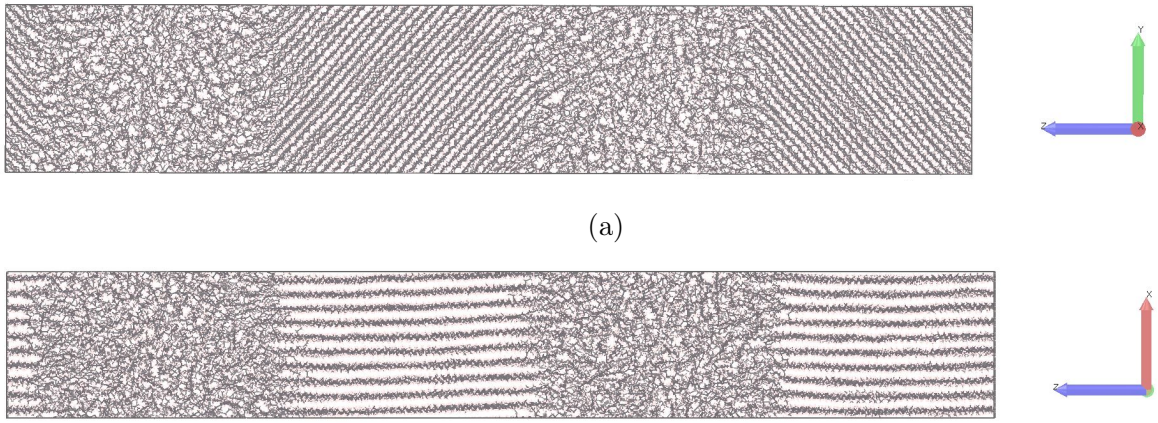

(a)

(b)

Figure 12: A structure seen from different directions: a. the y direction is vertical, b. the x direction is vertical.

x direction, essentially the weak non-covalent interactions oppose the deformation, when the structure is stretched along the y direction, there is a contribution of the stronger covalent interactions due to the tilt angle.

With the exception of the crystallinity ratio effect, we did not notice any correlation between the elastic coefficients and other morphological specificities such as the amount of tie chains or topological entanglements. Such behavior is expected in the small deformation regime.

3.3 High deformations

To investigate further the role of entanglements and molecular morphology, the structures were elongated with a strain rate $\dot{\epsilon} = 2.5 \cdot 10^{-3}$ ns^{-1} along the z axis from 0% to 50%. A strain of 0.5% per step was used followed by a relaxation in the NPT ensemble during 2 ns

at each step. The stress-strain curves obtained present a peak between 0.6 and 0.8% then a continuous decrease toward a plateau. Example of such curves can be found figure 13. A typical structure after 50% deformation is shown figure 14. We notice that after such

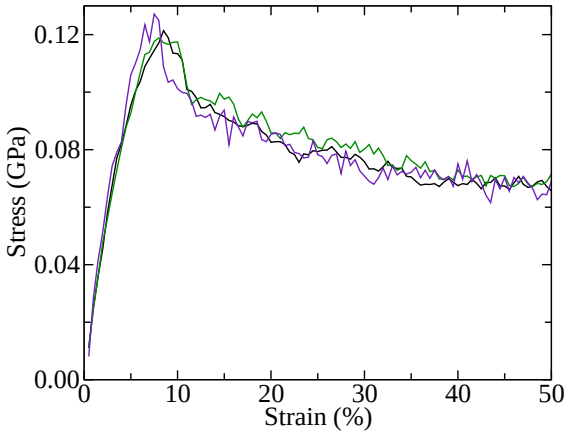

Figure 13: Stress-strain curve for the three structures with $\chi_{init} = 0.5$ and $C_\infty = 11$.

large stretching, crystalline phases are still present. The atoms which were initially in the crystalline phase (respectively in the amorphous phase) are colored in red (respectively in grey). One can notice that the stretching occurs by sliding of the chains. Several atoms previously in crystalline regions now appear in the amorphous phases and inversely. One amorphous region is almost destroyed, with the formation of a cavity and fibrils. This behavior is observed almost systematically in our samples.

What is considered to influence the mechanical properties are the so called *stress transmitters*.[36,59,62,66–68] The term encompasses bridging entanglements and tie chains. Bridging entanglements link polymer chains emerging from two different crystalline phases. We have considered here only loop-loop bridging entanglements, neglecting those including tail chains due to their small number.

To further investigate the high deformations, two criteria were used to characterize the stress-strain curves:

- the ultimate strength σ_{US} being the maximum stress the material withstands along the stress-strain curve,

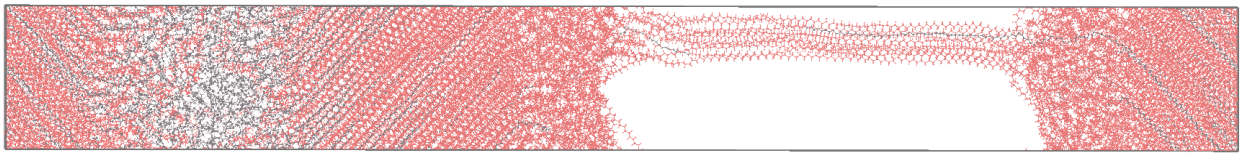

Figure 14: 50% stretched structure along the z direction. The red atoms are the atoms which were initially in the crystalline phase.

- the average stress from 25% to 50% strain, σ_{25-50}.

As shown figure 15, the ultimate strength σ_{US} and the average stress between 25 and 50% strain, σ_{25-50} are increasing with the crystallinity degree, as observed for the elastic coefficients c_{ii}. σ_{US} and σ_{25-50} are plotted figure 16 as a function of the number of tie chains

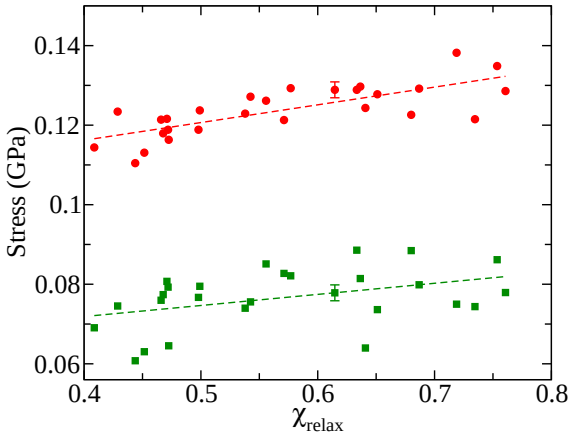

Figure 15: σ_{US} (red data) and σ_{25-50} (green data) as a function of the crystallinity degree χ_{relax}. Dashed lines are linear regressions of each data set. Error bars are stress fluctuations and are given on a single point.

and loop-loop bridging entanglements to investigate the importance of the *stress transmitters*. An increase of both stress quantities is expected with an increase of the number of stress transmitters. This increase is indeed observed for σ_{US} and σ_{25-50} versus the tie chain number. However, the opposite trend is observed versus loop-loop bridging entanglement number. The quantity of tie chains is the decisive factor over the entanglements to act as *stress transmitters*. This result confirms recent experimental work by McDermott.[69] It would be however interesting to quantitatively investigate the magnitude of loop-loop entanglements contribution. This implies to control the number of loop-loop entanglements

at constant number of other stress transmitters (tie chains). This is not possible as in our building procedure, $\bar{n}_{\text{tie}}$ and $\bar{n}_{\text{loop}}$ are not independent quantities (see figure 17). However when looking qualitatively at structures with the same amount of tie chains in each amorphous region, it is the region with the most loop-loop bridging entanglements which is the least deformed. The bridging entanglements are thus secondary *stress transmitters* behind the tie chains.

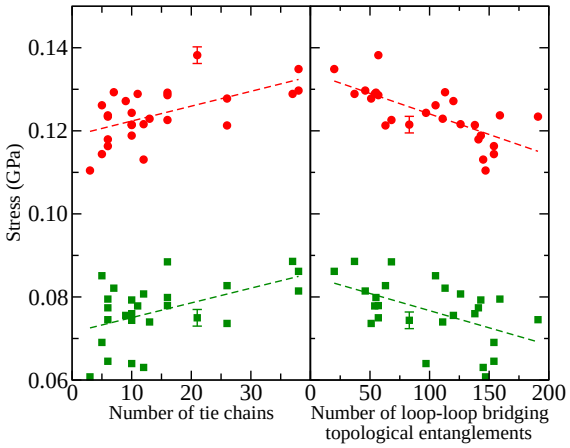

Figure 16: σ_{US} and σ_{25-50} as a function of the number of ties chains and loop-loop bridging topological entanglements. Error bars are stress fluctuations and are given on a single point.

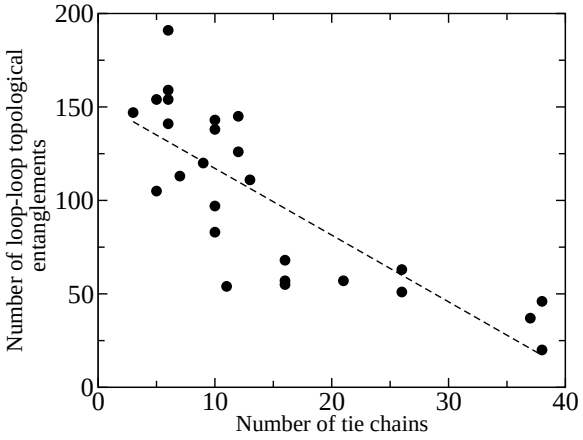

Figure 17: Relationship between the number of tie chains and loop-loop bridging entanglements.

4 Conclusion

This work presents a new modeling method for building atomistic semi-crystalline polymer models. Specifically, using a robust connection algorithm,[3] it was feasible to implement Adhikari's theory of tie chains, loops, and tails.[1] The crystallinity degree and the fraction of tie chains are adjustable degrees of freedom of the method. Although chain length distributions for ties, loops and tails are provided by the theory, different choices could be used to investigate limiting cases. Hence, structures with, for example, a high or low proportion of adjacent reentries could be modeled, as the one described by Nilsson.[43] When the methodology is applied to a model of semi-crystalline polyethylene, the initial constraints, i.e. the number of tie chains and the initial crystallinity degree, are well respected. Thus, the influence of these parameters onto morphological and mechanical properties can be studied. We observed that the density of topological entanglements in the amorphous regions is larger than the one observed in the melt, a result in agreement with Yoon and Flory[61] and Hoffman and Miller[60] theories. Also, this quantity is independent of the crystallinity ratio, though more studies would be needed to understand the relationship between topological entanglements and crystallinity ratio. The elastic coefficients are independent of the entanglements and the molecular morphology. This was shown by previous experimental work studies[70] and are mostly correlated with the crystallinity degree as expected from experimental studies.[65]

With this knowledge, computing semi-crystalline structure mechanical properties in the linear regime does not require controlling the fraction and distribution of the amorphous chains and the entanglement quantity but only the crystallinity degree. Thus a similar method to the one presented in this work with more simple analytical probability distributions may be sufficient to compute elastic coefficients.

For deformations far from the linear regime, the tie chains are the most critical stress transmitter; nevertheless, for structures with equal number of tie chains for both amorphous phases, the amorphous phase with the most bridging entanglements is the least deformed. The tie chains seem to be the primary *stress transmitters*, and the bridging entanglements

the secondary ones.

Acknowledgment

Martin Kröger (ETH Zurich) is acknowledged for providing us the Z1 code as well as advices for its use.

References

(1) Adhikari, S.; Muthukumar, M. Theory of Statistics of Ties, Loops, and Tails in Semicrystalline Polymers. *The Journal of Chemical Physics* **2019**, *151*, 114905.

(2) Theodorou, D. N.; Suter, U. W. Detailed Molecular Structure of a Vinyl Polymer Glass. *Macromolecules* **1985**, *18*, 1467–1478.

(3) Rigby, D.; Saxe, P. W.; Freeman, C. M.; Leblanc, B. In *Advanced Composites for Aerospace, Marine, and Land Applications*; Sano, T., Srivatsan, T. S., Peretti, M. W., Eds.; Springer International Publishing: Cham, 2016; pp 157–171.

(4) Birley, A. W. *Plastics Materials: Properties and Applications*; Springer Science & Business Media, 2012.

(5) Elias, H. G. *An Introduction to Plastics*; 1993.

(6) Schelten, J.; Ballard, D. G. H.; Wignall, G. D.; Longman, G.; Schmatz, W. Small-Angle Neutron Scattering Studies of Molten and Crystalline Polyethylene. *Polymer* **1976**, *17*, 751–757.

(7) Sadler, D. M.; Keller, A. Neutron Scattering Studies on the Molecular Trajectory in Polyethylene Crystallized from Solution and Melt. *Macromolecules* **1977**, *10*, 1128–1140.

(8) Schelten, J.; Wignall, G. D.; Ballard, D. G. H.; Longman, G. W. Small-Angle Neutron Scattering Studies of Molecular Clustering in Mixtures of Polyethylene and Deuterated Polyethylene. *Polymer* **1977**, *18*, 1111–1120.

(9) Stamm, M.; Fischer, E. W.; Dettenmaier, M.; Convert, P. Chain Conformation in the Crystalline State by Means of Neutron Scattering Methods. *Faraday Discussions of the Chemical Society* **1979**, *68*, 263–278.

(10) Spells, S. J.; Sadler, D. M. Neutron Scattering Studies on Solution-Grown Crystals of Polyethylene: A Statistical Preference for Adjacent Re-Entry. *Polymer* **1984**, *25*, 739–748.

(11) Ching, J. H. C.; Krimm, S. Mixed-crystal Infrared Studies on Melt-crystallized Polyethylene. *Journal of Applied Physics* **1975**, *46*, 4181–4184.

(12) Jing, X.; Krimm, S. Mixed-crystal Infrared Studies of Chain Folding in Polyethylene Single Crystals: Effect of Crystallization Temperature. *Journal of Polymer Science: Polymer Physics Edition* **1982**, *20*, 1155–1173.

(13) Cheam, T. C.; Krimm, S. Mixed-Crystal Infrared Studies of Chain-Folding in Polyethylene Single Crystals: Low-temperature and Molecular Weight Studies. *Journal of Polymer Science: Polymer Physics Edition* **1981**, *19*, 423–447.

(14) Reddy, K. R.; Tashiro, K.; Sakurai, T.; Yamaguchi, N. Cocrystallization Phenomenon between the H and D Species of Isotactic Polypropylene Blends As Revealed by Thermal and Infrared Spectroscopic Analyses for a Series of D/H Blend Samples. *Macromolecules* **2008**, *41*, 9807–9813.

(15) Kumaki, J.; Kawauchi, T.; Yashima, E. Two-Dimensional Folded Chain Crystals of a Synthetic Polymer in a Langmuir-Blodgett Film. *Journal of the American Chemical Society* **2005**, *127*, 5788–5789.

(16) Mullin, N.; Hobbs, J. K. Direct Imaging of Polyethylene Films at Single-Chain Resolution with Torsional Tapping Atomic Force Microscopy. *Physical Review Letters* **2011**, *107*, 197801.

(17) Savage, R. C.; Mullin, N.; Hobbs, J. K. Molecular Conformation at the Crystal–Amorphous Interface in Polyethylene. *Macromolecules* **2015**, *48*, 6160–6165.

(18) Hong, Y.-l.; Miyoshi, T. Chain-Folding Structure of a Semicrystalline Polymer in Bulk Crystals Determined by ^{13}C–^{13}C Double Quantum NMR. *ACS Macro Letters* **2013**, *2*, 501–505.

(19) Hong, Y.-l.; Chen, W.; Yuan, S.; Kang, J.; Miyoshi, T. Chain Trajectory of Semicrystalline Polymers As Revealed by Solid-State NMR Spectroscopy. *ACS Macro Letters* **2016**, *5*, 355–358.

(20) Esselink, K.; Hilbers, P. a. J.; van Beest, B. W. H. Molecular Dynamics Study of Nucleation and Melting of N-alkanes. *The Journal of Chemical Physics* **1994**, *101*, 9033–9041.

(21) Takeuchi, H. Structure Formation during the Crystallization Induction Period of a Short Chain-Molecule System: A Molecular Dynamics Study. *The Journal of Chemical Physics* **1998**, *109*, 5614–5621.

(22) Yi, P.; Rutledge, G. C. Molecular Simulation of Crystal Nucleation in N-Octane Melts. *The Journal of Chemical Physics* **2009**, *131*, 134902.

(23) Yi, P.; Rutledge, G. C. Molecular Simulation of Bundle-like Crystal Nucleation from n-Eicosane Melts. *The Journal of Chemical Physics* **2011**, *135*, 024903.

(24) Yi, P.; Locker, C. R.; Rutledge, G. C. Molecular Dynamics Simulation of Homogeneous Crystal Nucleation in Polyethylene. *Macromolecules* **2013**, *46*, 4723–4733.

(25) Zhang, W.; Larson, R. G. Direct All-Atom Molecular Dynamics Simulations of the Effects of Short Chain Branching on Polyethylene Oligomer Crystal Nucleation. *Macromolecules* **2018**, *51*, 4762–4769.

(26) Koyama, A.; Yamamoto, T.; Fukao, K.; Miyamoto, Y. Molecular Dynamics Simulation of Polymer Crystallization from an Oriented Amorphous State. *Physical Review. E, Statistical, Nonlinear, and Soft Matter Physics* **2002**, *65*, 050801.

(27) Lavine, M. S.; Waheed, N.; Rutledge, G. C. Molecular Dynamics Simulation of Orientation and Crystallization of Polyethylene during Uniaxial Extension. *Polymer* **2003**, *44*, 1771–1779.

(28) Ko, M. J.; Waheed, N.; Lavine, M. S.; Rutledge, G. C. Characterization of Polyethylene Crystallization from an Oriented Melt by Molecular Dynamics Simulation. *The Journal of Chemical Physics* **2004**, *121*, 2823–2832.

(29) Jabbarzadeh, A.; Tanner, R. I. Crystallization of Alkanes under Quiescent and Shearing Conditions. *Journal of Non-Newtonian Fluid Mechanics* **2009**, *160*, 11–21.

(30) Kavassalis, T. A.; Sundararajan, P. R. A Molecular-Dynamics Study of Polyethylene Crystallization. *Macromolecules* **1993**, *26*, 4144–4150.

(31) Liu, C.; Muthukumar, M. Langevin Dynamics Simulations of Early-Stage Polymer Nucleation and Crystallization. *The Journal of Chemical Physics* **1998**, *109*, 2536–2542.

(32) Hu, W. Chain Folding in Polymer Melt Crystallization Studied by Dynamic Monte Carlo Simulations. *The Journal of Chemical Physics* **2001**, *115*, 4395–4401.

(33) Meyer, H.; Müller-Plathe, F. Formation of Chain-Folded Structures in Supercooled Polymer Melts Examined by MD Simulations. *Macromolecules* **2002**, *35*, 1241–1252.

(34) Yamamoto, T. Molecular Dynamics Simulations of Steady-State Crystal Growth and Homogeneous Nucleation in Polyethylene-like Polymer. *The Journal of Chemical Physics* **2008**, *129*, 184903.

(35) Yamamoto, T. Molecular Dynamics Simulations of Polymer Crystallization in Highly Supercooled Melt: Primary Nucleation and Cold Crystallization. *The Journal of Chemical Physics* **2010**, *133*, 034904.

(36) Jabbari-Farouji, S.; Lame, O.; Perez, M.; Rottler, J.; Barrat, J.-L. Role of the Intercrystalline Tie Chains Network in the Mechanical Response of Semicrystalline Polymers. *Physical Review Letters* **2017**, *118*, 217802.

(37) Balijepalli, S.; Rutledge, G. C. Simulation Study of Semi-Crystalline Polymer Interphases. *Macromolecular Symposia* **1998**, *133*, 71–99.

(38) Gautam, S.; Balijepalli, S.; Rutledge, G. C. Molecular Simulations of the Interlamellar Phase in Polymers: Effect of Chain Tilt. *Macromolecules* **2000**, *33*, 9136–9145.

(39) Balijepalli, S.; Rutledge, G. C. Conformational Statistics of Polymer Chains in the Interphase of Semi-Crystalline Polymers. *Computational and Theoretical Polymer Science* **2000**, *10*, 103–113.

(40) Rutledge, G. C. Implications of Metastability for the Crystal/Amorphous Interface from Molecular Simulation. *Journal of Macromolecular Science, Part B* **2002**, *41*, 909–922.

(41) in 't Veld, P. J.; Rutledge, G. C. Temperature-Dependent Elasticity of a Semicrystalline Interphase Composed of Freely Rotating Chains. *Macromolecules* **2003**, *36*, 7358–7365.

(42) P. J. Veld, I. T.; Hütter, M.; Rutledge, G. C. Temperature-Dependent Thermal and Elastic Properties of the Interlamellar Phase of Semicrystalline Polyethylene by Molecular Simulation. *Macromolecules* **2006**, *39*, 439–447.

(43) Nilsson, F.; Lan, X.; Gkourmpis, T.; Hedenqvist, M.; Gedde, U. Modelling Tie Chains and Trapped Entanglements in Polyethylene. *Polymer* **2012**, *53*, 3594–3601.

(44) Pandiyan, S.; Rousseau, B. Factors Influencing Properties of Interfacial Regions in Semicrystalline Polyethylene: A Molecular Dynamics Simulation Study. *Polymer* **2013**, *54*, 3586–3593.

(45) Monasse, B.; Queyroy, S.; Lhost, O. Molecular Dynamics Prediction of Elastic and Plastic Deformation of Semi-Crystalline Polyethylene. *International Journal of Material Forming* **2008**, *1*, 1111–1114.

(46) Queyroy, S.; Monasse, B. Effect of the Molecular Structure of Semicrystalline Polyethylene on Mechanical Properties Studied by Molecular Dynamics. *Journal of Applied Polymer Science* **2012**, *125*, 4358–4367.

(47) Guttman, C. M.; DiMarzio, E. A.; Hoffman, J. D. Modelling the Amorphous Phase and the Fold Surface of a Semicrystalline Polymer—the Gambler's Ruin Method. *Polymer* **1981**, *22*, 1466–1479.

(48) Bunn, C. W. The Crystal Structure of Long-Chain Normal Paraffin Hydrocarbons. The "Shape" of The. *Transactions of the Faraday Society* **1939**, *35*, 482–491.

(49) Rubinstein, M. *Polymer Physics*; Oxford University Press: Oxford ;, 2007.

(50) Flory, P. J. *Statistical Mechanics of Chain Molecules*; Hanser Gardner Pubns, 1989.

(51) Devroye, L. In *Non-Uniform Random Variate Generation*; Devroye, L., Ed.; Springer: New York, NY, 1986; pp 27–82.

(52) Materials Design, Inc., MedeA 3.4, Materials Exploration and Design Analysis. `https://materialsdesign.com`.

(53) Thompson, A. P.; Aktulga, H. M.; Berger, R.; Bolintineanu, D. S.; Brown, W. M.; Crozier, P. S.; in 't Veld, P. J.; Kohlmeyer, A.; Moore, S. G.; Nguyen, T. D. et al.

LAMMPS - a flexible simulation tool for particle-based materials modeling at the atomic, meso, and continuum scales. *Comp. Phys. Comm.* **2022**, *271*, 108171.

(54) Martin, M. G.; Siepmann, J. I. Transferable Potentials for Phase Equilibria. 1. United-Atom Description of n-Alkanes. *The Journal of Physical Chemistry B* **1998**, *102*, 2569–2577.

(55) Lange, N. A.; Speight, J. G. *Lange's Handbook of Chemistry / Edited by J. G. Speight..*, 16th ed.; McGraw-Hill Professional: New York ; London, 2005.

(56) Kröger, M. Shortest Multiple Disconnected Path for the Analysis of Entanglements in Two- and Three-Dimensional Polymeric Systems. *Computer Physics Communications* **2005**, *168*, 209–232.

(57) Ranganathan, R.; Kumar, V.; Brayton, A. L.; Kröger, M.; Rutledge, G. C. Atomistic Modeling of Plastic Deformation in Semicrystalline Polyethylene: Role of Interphase Topology, Entanglements, and Chain Dynamics. *Macromolecules* **2020**, *53*, 4605–4617.

(58) Shanbhag, S.; Kröger, M. Primitive Path Networks Generated by Annealing and Geometrical Methods: Insights into Differences. *Macromolecules* **2007**, *40*, 2897–2903.

(59) Lee, S.; Rutledge, G. C. Plastic Deformation of Semicrystalline Polyethylene by Molecular Simulation. *Macromolecules* **2011**, *44*, 3096–3108.

(60) Hoffman, J. D.; Miller, R. L. Kinetic of Crystallization from the Melt and Chain Folding in Polyethylene Fractions Revisited: Theory and Experiment. *Polymer* **1997**, *38*, 3151–3212.

(61) Flory, P. J.; Yoon, D. Y. Molecular Morphology in Semicrystalline Polymers. *Nature* **1978**, *272*, 226–229.

(62) Bartczak, Z. Evaluation of Effective Density of the Molecular Network and Concentration of the Stress Transmitters in Amorphous Layers of Semicrystalline Polyethylene. *Polymer Testing* **2018**, *68*, 261–269.

(63) Hoy, R. S.; Foteinopoulou, K.; Kröger, M. Topological Analysis of Polymeric Melts: Chain-length Effects and Fast-Converging Estimators for Entanglement Length. *Physical Review E* **2009**, *80*, 031803.

(64) Ramos, J.; Vega, J. F.; Theodorou, D. N.; Martinez-Salazar, J. Entanglement Relaxation Time in Polyethylene: Simulation versus Experimental Data. *Macromolecules* **2008**, *41*, 2959–2962.

(65) Addiego, F.; Dahoun, A.; G'Sell, C.; Hiver, J.-M.; Godard, O. Effect of Microstructure on Crazing Onset in Polyethylene under Tension. *Polymer Engineering & Science* **2009**, *49*, 1198–1205.

(66) Seguela, R. Critical Review of the Molecular Topology of Semicrystalline Polymers: The Origin and Assessment of Intercrystalline Tie Molecules and Chain Entanglements. *Journal of Polymer Science Part B: Polymer Physics* **2005**, *43*, 1729–1748.

(67) Takayanagi, M.; Nitta, K.-h. Application of a Tie Molecule Model to the Postyielding Deformation of Crystalline Polymers. *Macromolecular Theory and Simulations* **1997**, *6*, 181–195.

(68) Moyassari, A.; Mostafavi, H.; Gkourmpis, T.; Hedenqvist, M. S.; Gedde, U. W.; Nilsson, F. Simulation of Semi-Crystalline Polyethylene: Effect of Short-Chain Branching on Tie Chains and Trapped Entanglements. *Polymer* **2015**, *72*, 177–184.

(69) McDermott, A. G.; DesLauriers, P. J.; Fodor, J. S.; Jones, R. L.; Snyder, C. R. Measuring Tie Chains and Trapped Entanglements in Semicrystalline Polymers. *Macromolecules* **2020**, *53*, 5614–5626.

(70) Bartczak, Z. Effect of Chain Entanglements on Plastic Deformation Behavior of Linear Polyethylene. *Macromolecules* **2005**, *38*, 7702–7713.